Anomalous optical and electronic properties of dense sodium

A. Lazicki[a,1], A. F. Goncharov[a], V. V. Struzhkin[a], R. E. Cohen[a], Z. Liu[a], E. Gregoryanz[b], C. Guillaume[b], H.-K. Mao[a], and Russell J. Hemley[a,1]

[a]Geophysical Laboratory, Carnegie Institution of Washington, Washington, D.C. 20015; and [b]Scottish Universities Physics Alliance, School of Physics and Centre for Science at Extreme Conditions, University of Edinburgh, Edinburgh EH9 3JZ, United Kingdom

Contributed by Russell J. Hemley, February 24, 2009 (sent for review February 19, 2009)

Synchrotron infrared spectroscopy on sodium shows a transition from a high reflectivity, nearly free-electron metal to a low-reflectivity, poor metal in an orthorhombic phase at 118 GPa. Optical spectra calculated within density functional theory (DFT) agree with the experimental measurements and predict a gap opening in the orthorhombic phase at compression beyond its stability field, a state that would be experimentally attainable by appropriate choice of pressure-temperature path. We show that a transition to an incommensurate phase at 125 GPa results in a partial recovery of good metallic character up to 180 GPa, demonstrating the strong relationship between structure and electronic properties in sodium.

high pressure | infrared reflectivity | metal-insulator transition

The alkali metals are often presented as textbook examples of simple metals. At low pressures they all take on very simple bcc and fcc crystal structures and display the free-electronlike metallic character predictable for monovalent compounds (1). However, recent work has shown that the application of pressure results in an unexpected variety of complex phenomena. These include the existence of low-symmetry and even incommensurate phases (2–10) and significant electronic changes leading to effects such as unusual melting behavior (10), Fermi-surface nesting (11), phonon instabilities (12), electron-phonon coupling and superconductivity (13,14), and transformations to poor metals or even insulators (9, 15–18). Sodium is unique among the alkali metals because of its occupied electronic states; it differs from lithium by the presence of p states, and from the heavier alkalis by the absence of d states under compression. Its Fermi surface remains spherical up to 120 GPa, whereas in all other alkali metals the Fermi surface is significantly deformed by 7 GPa (12). It is the only alkali metal not predicted to date to become a superconductor under pressure (14). It exhibits the largest pressure-induced drop in melting temperature ever reported, dropping from ≈1,000 K to nearly room temperature at 120 GPa (10), and possessing crystal structures in the vicinity of the melting minimum with hundreds of atoms per unit cell (8). It has been suggested that an observed darkening of the metal (18) at a transition to an incommensurate phase at 125 GPa may signify the onset of semiconducting or insulating behavior suggested in theoretical studies for sodium (15,16). To address this, we have conducted synchrotron and conventional reflectivity measurements on sodium metal in the low-symmetry phases up to ≈180 GPa and performed first-principles calculations on the reported crystal structures. We demonstrate that a transition to an orthorhombic phase is accompanied by near-insulating behavior and find that further (metastable) compression of this phase would result in a metal-insulator transition. Enhanced metallic behavior is partially recovered, however, in the incommensurate phase, in which valence charge density accumulates into quasi 1-dimensional channels within the crystal structure, resulting in highly anisotropic metallic character.

Results and Discussion

At ambient temperature, the expected sequence of crystal structures in sodium is as follows: bcc, 0 → 65 GPa; fcc, 65 → 105 GPa; cI16, 105 → 118 GPa (5); oP8, 118 → 125 GPa (8); and tI19, 125 → 155+ GPa (18). Experimental synchrotron IR reflectivity was collected up to ≈180 GPa in a diamond anvil cell in these 5 phases (Fig. 1), and modeled at the sample-diamond interface with first-principles density functional theory. Dielectric and optical properties are obtained from experimental reflectivity spectra (Fig. 2) with the classical oscillator model. We have fit the free carrier contribution with the Drude model and the interband absorption contributions with Lorentz oscillators. We found good agreement between experimental results and theoretical predictions.

Reflectivity is high and uniform across the energy range examined for the bcc and fcc phases. Optical properties undergo only subtle changes with pressure in these phases up to 105 GPa, similar to those documented for other alkali metals (19,20). This is consistent with the free-electron-like behavior already known for sodium in these phases.

In 2 of the 4 experiments, the reflectivity in the cI16 phase was ≈15% lower. This change is barely larger than the standard error in our measurements, so may not have been detectable in half the experiments. Calculations predict a drop in reflectivity due to electronic absorption between closely-spaced parallel energy bands between N and Γ (Fig. 3), which give rise to an interband feature in the optical conductivity at ≈0.5 eV. A small pseudogap opening at the Fermi level is observed (Fig. 4), resulting from a transfer of electrons from s states to p states. Such a gap has been observed in the same phase in lithium, and is suggested to be the source of energetic stability for this phase.

At the transition to the oP8 phase at 118 GPa, there is a distinct drop in reflectivity over the entire energy range measured. We also observe a visible loss of luster in the sample at this pressure (Fig. 1 *Inset*). The measured drop in reflectivity in the visible regime is higher than theoretically predicted (Fig. 2), a discrepancy that may result from the typical underestimation of energy gaps in the LDA and consequent errors in estimation of absorption energies. The calculated results of electronic properties are in excellent agreement with those of Lundegaard et al. (18), and display the existence of an extended network of parallel bands in this semimetallic phase, leading to interband absorption throughout the visible regime. The calculated plasma frequency (Fig. 5) also dropped into the visible range in this phase (ω_p = 1.7 eV, averaged over the 3 crystallographic directions), reflecting the decreased density of free carriers. The oP8 phase exists over a very narrow pressure range. However, if the volume is scaled down with the lattice parameter ratios and internal parameters kept fixed, the pseudogap increases and a metal-insulator transition would occur by $V/V_0 \approx 20\%$ (≈200

Author contributions: A.L., A.F.G., V.V.S., R.E.C., E.G., H.-K.M., and R.J.H. designed research; A.L. and Z.L. performed research; V.V.S., Z.L., E.G., and C.G. contributed new reagents/analytic tools; A.L., A.F.G., V.V.S., R.E.C., and Z.L. analyzed data; and A.L. and R.J.H. wrote the paper.

The authors declare no conflict of interest.

[1]To whom correspondence may be addressed. E-mail: alazicki@ciw.edu or hemley@gl.ciw.edu.

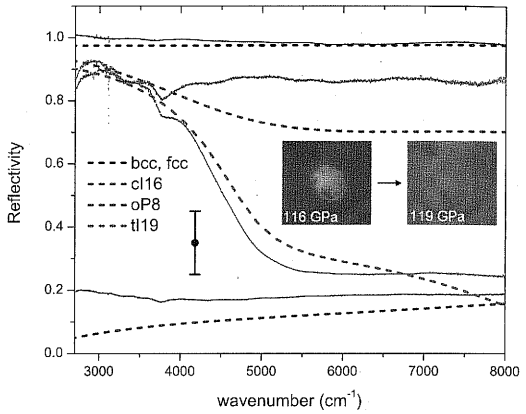

Fig. 1. Reflectivity in the known ambient-temperature phases of Na (bcc and fcc are essentially identical) from experiments (solid lines) and our first-principles density functional theory computations (dashed lines). Experimental data shown are representative spectra. Average error in experimental data (as a result of difficulties in modeling diamond absorption and other effects such as surface inhomogeneities on the sample and references) is shown with the error bar. Broad features, however, are consistent in all experiments. An image of a sample across the cI16 → oP8 transition is shown (pressure measured from ruby fluorescence).

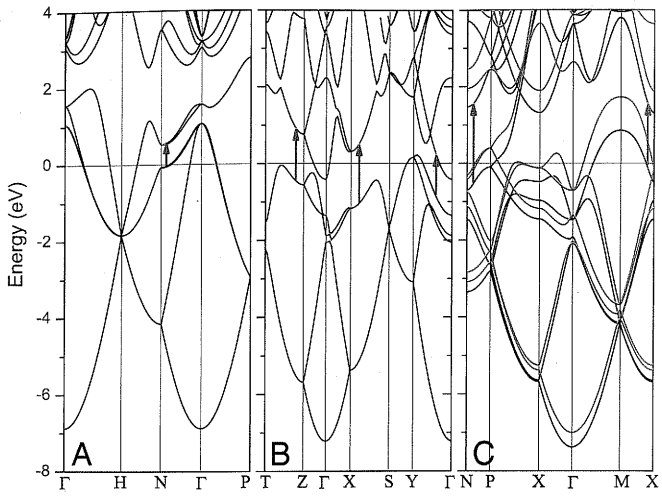

Fig. 3. Electronic bandstructure for cI16 at 113 GPa (*A*), oP8 at 119 GPa (*B*), and "tI19" at 147 GPa (*C*). In *C*, the black curve corresponds to the tI20 model with guest atoms in the 2b or 2d sites of the I4/mcm space group, and the red curve corresponds to the tI18 model with guest atoms in the 2c site. The blue arrows illustrate paths for interband electronic transitions.

GPa). This is much lower in pressure than the predicted zero gap semiconductor of Neaton et al. (15) at $V/V_0 \approx 13\%$ or 800 GPa, indicating a highly sensitive relationship between structure and electronic properties in sodium. The gap opening is related to the onset of more covalent bonding, leading to splitting of bonding and antibonding states. The strongly sp hybridized band with its minimum at the Γ point rises rapidly with pressure, opening an indirect gap that continues to widen upon further compression. The increasingly covalent character can also be seen from the presence of preferentially closer interatomic distances in the oP8 phase, and the strong relationship between structure and electronic properties. We also observe a buildup of valence charge density in the interstitial regions of the crystal lattice due to Pauli exclusion and orthogonality. The displaced charge forms isolated oblong regions with a bimodal distribution (Fig. 6), as also

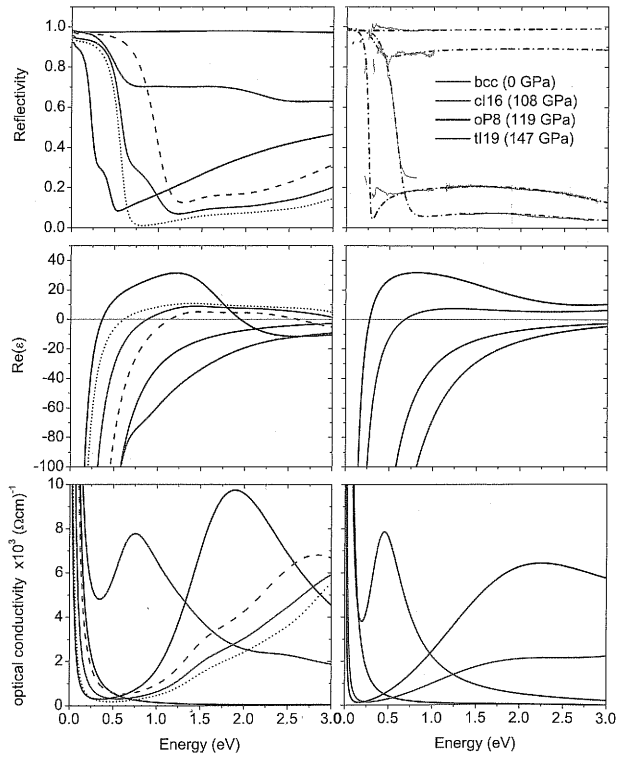

Fig. 2. Reflectivity, real part of the dielectric constant and optical conductivity of Na in the bcc, cI16, oP8 and tI19 phases from theoretical calculations (left column) and Lorentz oscillator fits to experimental reflectivity data (right column). Oscillator fits to reflectivity are shown as dash-dot lines to distinguish them from experimental reflectivity data. The components of optical properties calculated for the "tI19" phase along different crystallographic directions are shown as the dotted curve (*xy* component) and dashed curve (*z* component), with the average as the solid curve.

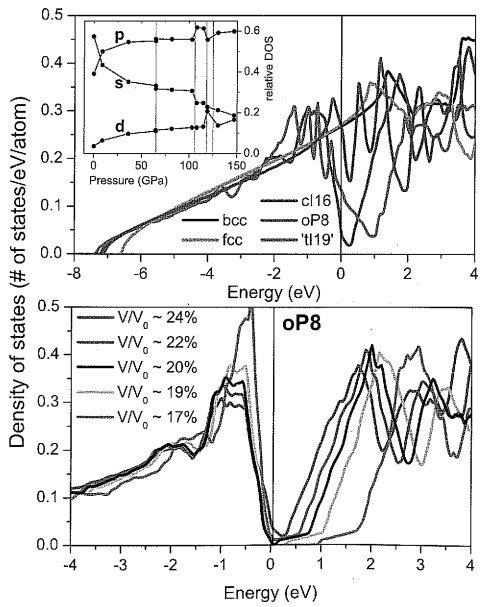

Fig. 4. Density of electronic states. (*Upper*) The 5 phases of Na: bcc (65 GPa), fcc (65 GPa), cI16 (115 GPa), oP8 (119 GPa) and "tI19" (147 GPa). (*Inset*) Evolution of the projected density of states relative to total density of states at the Fermi level as a function of pressure. Note that tails of states of neighboring atoms appear partially as d-character; thus the rise in d character is due mainly to shorter near-neighbor distances. (*Lower*) Density of states in the oP8 phase at compressed volume. V_0 refers to atomic volume at ambient pressure.

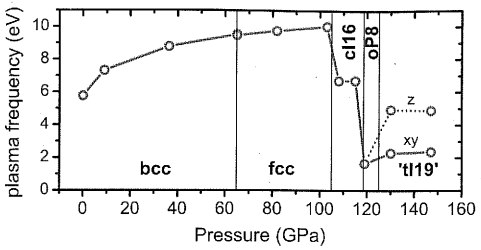

Fig. 5. Theoretically calculated change in plasma frequency in the 5 known phases. The values along different crystallographic directions are shown for the "tI19" phase.

predicted for lithium (21). Insulating oP8 Na may be achieved experimentally if the oP8 phase can be compressed metastably. The technique of trapping phases outside of their stability fields by choosing an appropriate pressure-temperature path and compression rate is becoming increasingly common (22, 23).

The reflectivity in the visible energy range drops still further at the transition to the tI19 phase. However, in the IR regime, high reflectivity is recovered <0.75 eV, proving that sodium does not become an insulator at this transition. We conclude based on the good reproduction by the theoretical model of the dominant feature in the reflectivity spectrum that our approximation to the incommensurate phase may yield useful electronic information. The rise in reflectivity at low energy is due to the shift in interband absorption to higher energy. The band minima between 1 and 2.5 eV, which have significant s character, are continuing to rise in energy relative to the mostly p-like upper valence bands as the density gets higher, leading to higher energy absorption. There is a large increase in the plasma frequency in the z polarization direction (ω_{pz} = 4.94 eV) whereas the in the xy-direction (ω_{pxy} = 2.15 eV) it changes very little from the oP8 phase (Fig. 5). The optical properties are quite anisotropic (Fig. 2), suggesting an enhanced free-carrier mobility along z. As in the oP8 phase, we see an accumulation of valence charge density in the interstitial regions. Here, it takes the form of periodically modulated columns along z, passing through the center of the unit cell (Fig. 6). A proportionate scaling down of the volume in this structure did not result in an insulating phase, as in oP8, up to the highest volume reduction examined (V/V_0 ≈18%). The band maximum at the M point (composed of predominantly p and d character of the "guest" atoms) falls in energy as density increases, but a gap is unlikely to open because of the valence band crossing the Fermi level at the P point (which has a mixture of host and guest p character), where it is degenerate with an occupied p band. Whether the monoclinic distortion of the guest lattice may lift the band degeneracy at the Fermi level at P and open a gap at higher density remains to be examined. Experimentally, the reflectivity of tI19 Na remains unchanged (within the precision of our experimental data) up to ≈180 GPa.

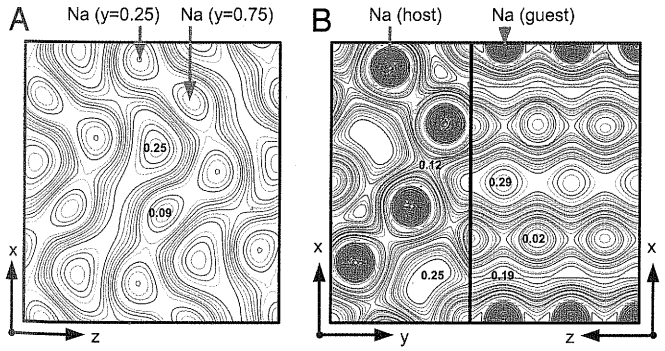

Fig. 6. Charge density from partially occupied bands in the xz plane of the oP8 phase at y = 0.5 between layers of sodium atoms (A) and the xy plane at z = 0.5 (*Left*) and the yz plane at x = 0.5 (*Right*) of the "tI19" phase (B). Contour lines are separated by 0.01 e/Å^3

Conclusions

In conclusion, we have demonstrated experimentally a dramatic decrease in IR reflectivity of sodium at the onset of the oP8 phase transition at 118 GPa, due to absorption between parallel energy bands, which are fully gapped across the Brillouin zone. Splitting of bonding and antibonding-type hybridized energy bands results in an indirect gap opening at a 5-fold volume reduction, beyond the stability regime of this phase. The possibility of metastable compression of this phase by appropriate choice of P–T path to achieve the insulating state is worth investigation. Low energy reflectivity is recovered in the incommensurate phase, in which optical properties are distinctly anisotropic. Heightened carrier mobility along z is suggested to be due to the presence of 1D columns of valence charge accumulated in the open channels along z due to exclusion of s and p-like states from the regions of strong core overlap. Sodium in the tI19 phase remains metallic up to at least 180 GPa. Metallic character is shown to be highly sensitive to crystal structure in sodium. Further high pressure phase transitions are likely to result in significant changes; whether the metal-insulator transition will occur remains difficult to predict.

Methods

Experimental. Sodium was loaded into diamond anvil cells under an inert argon atmosphere without a pressure medium. Ruby chips were used as a pressure indicator up to ≈100 GPa, after which pressure was estimated from the shift in the first-order diamond raman mode (24). Type 1A diamonds with 300/100 bevels and rhenium gaskets with ≈60-μm sample sizes were used to attain pressures of ≈180 GPa. Consistent results were obtained from 4 separate experiments. Synchroton IR spectra were collected at beamline U2A of the National Synchrotron Light Source at Brookhaven National Laboratory. An aperture size of ≈20 × 20 μm allowed the exclusion of scattering from the surrounding gasket. Reflectivity <0.5 eV was limited by absorption from nitrogen impurities in the diamond. The procedure used to calculate values for reflectivity at the sample-diamond interface is outlined in ref. 25. Corrections for absorption in the diamond were made by measuring reflectivity from the back and culet of a diamond in an empty cell and spectra were referenced to reflectivity collected from the back of the diamond at each pressure point, assuming standard values for diamond reflectivity and transmission (26). Visible and near-IR reflectivity were also collected to access the 0.5 → 3 eV energy range. Data were fit with classical Lorentz oscillators, including a zero-frequency free-carrier Drude contribution. In the bcc, fcc, and cI16 phases the plasma frequency was outside of the range of experimental data collected and thus could not be determined from measurements alone. In the high pressure phases, the effects of decreasing plasma frequency and emerging contributions from interband absorption could not be decoupled. As a result, theoretically calculated values for plasma frequency were used as a starting point for our data fitting, and it was necessary to introduce 1 Lorentz oscillator in the cI16 phase and 2 in the oP8 and tI19 phases to reach reasonable agreement with experimental spectra.

Theoretical. First-principles calculations were performed on the experimentally reported crystal structures, using the WIEN2k LAPW code (27). We used the GGA exchange correlation energy functional of Perdew and Wang (28), and found well-converged results with ≈200 (exact value depended on symmetry) irreducible k points and $R \times K_{max}$ (the muffin tin radius multiplied by the maximum k in the expansion of the plane wave basis set) = 9. Density of states and bandstructures were obtained in this manner. In the complex high pressure phases, the lattice parameters and internal coordinates were not "relaxed" to the minimum energy values but rather taken directly from the experimental results. Optical properties were calculated based on the random phase approximation (RPA) using the formulation of Ambrosch-Draxl (29). A much finer mesh of k points is required for this method and we have used ≈5,000 k points in the irreducible wedge. This method has been shown to be quite accurate for good metals because the effective screening of the core

PHYSICS

electrons is required for the RPA. At high pressures where the material may be a poor metal, the results are potentially less reliable. The high pressure incommensurate phase (tI19) was modeled by considering the most closely related commensurate phases: "tI20"—the I4/mcm host lattice with guest atoms occupying the 2b or 2d sites, yielding a tetragonal guest lattice with c_{guest} 17% reduced from the experimental value and "tI18"—an I-4 host lattice with guest atoms in the 2c site, yielding a c_{guest} 60% larger. The dominant features of the electronic structure near the Fermi level are not significantly effected by position and separation distance of the guest atoms (as shown in Fig. 4C). The good agreement with experimental results indicates that the reported monoclinic distortion of the guest lattice (18) will also not greatly change the electronic structure. The calculated electronic and optical properties shown for tI19 Na in this article are those of the "tI20" unmodulated structure with guest atoms in the 2b site.

ACKNOWLEDGMENTS. We thank M. Weinberger for help with the experiments and critical reading of the manuscript; L. Shulenburger and P. Ganesh for helpful discussions; and C. S. Yoo, C. T. Seagle, M. Guthrie, W. E. Pickett, J. J. Dong and G. P. Williams for useful comments. This work was supported by U.S. National Science Foundation Grants DMR 0805056 and EAR 0711358, and the Balzan Foundation. The U2A beamline is supported by the Consortium for Materials Properties Research in Earth Sciences under National Science Foundation Cooperative Agreement 06-49658; U.S. Department of Energy Basic Energy Sciences and National Nuclear Security Administration/Carnegie-Department of Energy Alliance Center) grant number DE-FC52-08NA28554. Use of the National Synchrotron Light Source, Brookhaven National Laboratory, was supported by the U.S. Department of Energy, Office of Science, Office of Basic Energy Sciences, under Contract DE-AC02-98CH10886. E.G. and C.G. were supported by a research grant from the U.K. Engineering and Physical Sciences Research Council.

1. Wigner E, Seitz F (1933) On the constitution of metallic sodium. *Phys Rev* 43:804–810.
2. Hanfland M, Syassen K, Christensen NE, Novikov DL (2000) New high-pressure phases of lithium. *Nature* 408:174–178.
3. Nelmes RJ, McMahon MI, Loveday JS, Rekhi S (2002) Structure of Rb-III: Novel modulated stacking structures in alkali metals. *Phys Rev Lett* 88:155503–155507.
4. McMahon MI, Nelmes RJ, Rekhi S (2001) Complex crystal structure of cesium-III. *Phys Rev Lett* 87:255502–255506.
5. McMahon MI, et al. (2007) Structure of sodium above 100 GPa by single-crystal x-ray diffraction. *PNAS* 104:17297–17299.
6. McMahon MI, Nelmes RJ (2004) Chain "melting" in the composite Rb-IV structure. *Phys Rev Lett* 93:055501–055505.
7. McMahon MI, Nelmes RJ, Schwarz U, Syassen K (2006) Composite incommensurate K-III and a commensurate form: Study of a high-pressure phase of potassium. *Phys Rev B* 74:140102–140106(R) (2006).
8. Gregoryanz E, et al. (2008) Structural diversity of sodium. *Science* 320:1054–1057.
9. Goncharov AF, Struzhkin VV, Mao H-K, Hemley RJ (2005) Spectroscopic evidence for broken-symmetry transitions in dense lithium up to megabar pressures. *Phys Rev B* 71:184114–184120.
10. Gregoryanz E, Degtyareva O, Somayazulu M, Hemley RJ, Mao H-K (2005) Melting of dense sodium. *Phys Rev Lett* 94:185502–185506.
11. Rodriguez-Prieto A, Bergara A, Silkin VM, Echenique PM (2006) Complexity and Fermi surface deformation in compressed lithium. *Phys Rev B* 74:172104–172108.
12. Xie Y, et al. (2008) Origin of bcc to fcc phase transition under pressure in alkali metals. *New J Phys* 10:063022.
13. Shimizu K, Ishikawa H, Takao D, Yagi T, Amaya K (2002) Superconductivity in compressed lithium at 20 K. *Nature* 419:597–599.
14. Shi L, Papaconstantopoulos DA (2006) Theoretical predictions of superconductivity in alkali metals under high pressure. *Phys Rev B* 73:184516–184521.
15. Neaton JB, Ashcroft NW (2001) On the constitution of sodium at higher densities. *Phys Rev Lett* 86:2830–2833.
16. Christensen NE, Novikov DL (2001) High-pressure phases of the light alkali metals. *Solid State Commun* 119:477–490.
17. Bastea M, Bastea S (2002) Electrical conductivity of lithium at megabar pressures. *Phys Rev B* 65:193104–193108.
18. Lundegaard LF, et al. (2009) Single-crystal studies of incommensurate Na to 1.5 Mbar. *Phys Rev B* 79:064105–064110.
19. Takemura K, Syassen K (1983) High-pressure phase transitions in potassium and phase relations among heavy alkali metals. *Phys Rev B* 28:1193–1196.
20. Alouani M, Christensen NE, Syassen K (1989) Calculated ground-state and optical properties of potassium under pressure. *Phys Rev B* 39:8096–8106.
21. Neaton JB, Ashcroft NW (1999) Pairing in dense lithium. *Nature* 400:141–144.
22. Eremets MI, Hemley RJ, Mao H-K, Gregoryanz E (2001) Semiconducting non-molecular nitrogen up to 240 GPa and its low-pressure stability. *Nature* 411:170–174.
23. Klotz S, *et al.* (1999) Metastable ice VII at low temperature and ambient pressure. *Nature* 398:681–684.
24. Eremets MI (2003) Megabar high-pressure cells for Raman measurements. *J Raman Spectrosc* 34:515–518.
25. Seagle CT, Heinz DL, Liu Z, Hemley RJ (2009) Synchrotron infrared reflectivity measurements of iron at high pressures. *Appl Opt* 48:545–552.
26. Zaitsev AM (2001) *Optical Properties of Diamond: A Data Handbook* (Springer, Berlin), pp 13–16.
27. Blaha P, Schwarz K, Madsen G, Kvasnicka D, Luitz J (2001) *WIEN2k* an augmented plane wave + local orbitals program for calculating crystal properties (Technische Universität Wien, Vienna).
28. Perdew JP, Burke K, Ernzerhof M (1996) Generalized gradient approximation made simple. *Phys Rev Lett* 77:3865–3868.
29. Ambrosch-Draxl C, Sofo JO (2006) Linear optical properties of solids within the full-potential linearized augmented planewave method. *Comp Phys Comm* 175:1–14.